

METALLICITY EFFECTS ON MID-INFRARED COLORS AND THE 8 μ m PAH EMISSION IN GALAXIES

C. W. ENGELBRACHT¹, K. D. GORDON¹, G. H. RIEKE¹, M. W. WERNER², D. A. DALE³, AND W. B. LATTER⁴

Draft version July 18, 2018

ABSTRACT

We examine colors from 3.6 μ m to 24 μ m as a function of metallicity (O/H) for a sample of 34 galaxies. The galaxies range over 2 orders of magnitude in metallicity. They display an abrupt shift in the 8 μ m to 24 μ m color between metallicities 1/3 to 1/5 of the solar value. The mean 8 μ m to 24 μ m flux density ratio below and above $12 + \log(O/H) = 8.2$ is 0.08 ± 0.04 and 0.70 ± 0.53 , respectively. We use mid-infrared colors and spectroscopy to demonstrate that the shift is primarily due to a decrease in the 8 μ m flux density as opposed to an increase in the 24 μ m flux density. This result is most simply interpreted as due to a weakening at low metallicity of the mid-infrared emission bands usually attributed to PAHs (polycyclic aromatic hydrocarbons) relative to the small-grain dust emission. However, existing empirical spectral energy distribution models cannot account for the observed short-wavelength (i.e., below 8 μ m) colors of the low-metallicity galaxies merely by reducing the strength of the PAH features; some other emission source (e.g., hot dust) is required.

Subject headings: galaxies: ISM—infrared: galaxies

1. INTRODUCTION

Early galaxies must have formed at a very low metallicity. Such galaxies likely had different properties from typical galaxies observed in the local universe, where generations of star formation have enriched the ISM (interstellar medium). These early galaxies are difficult to study because they are so distant. As a result, nearby low-metallicity galaxies have generated considerable interest as local analogs of young galaxies at high redshift (see, for example, the review by Kunth & Östlin 2000).

Understanding the infrared properties of nearby low metallicity galaxies will help guide interpretation of *Spitzer* observations of high-redshift ones (e.g., Fazio et al. 2004; Yan et al. 2004; Lagache et al. 2004). An important aspect of infrared galaxy spectral energy distributions (SEDs) is the behavior between 3 and 24 μ m, a range that includes emission from PAH (Polycyclic Aromatic Hydrocarbon) molecules and warm dust. At redshifts between 1 and 3, the PAH features move through the MIPS 24 μ m band. *Ad hoc* adjustments to this spectral region in SED models (Lagache et al. 2004) have been required to fit the 24 μ m number counts (Papovich et al. 2004; Marleau et al. 2004; Chary et al. 2004). Liang et al. (2004) show that infrared luminous galaxies at $z \sim 0.6$ are only $\sim 50\%$ as metal-rich as their local analogs. Therefore, interpreting the behavior of galaxies detected with *Spitzer* to substantially higher redshifts (e.g., Pérez-González et al. 2005, submitted to ApJ) depends critically on understanding the effects of metallicity on the 24 μ m flux densities for $1 < z < 3$.

Low-metallicity galaxies are difficult to find: I Zw 18, the first extreme example identified (Searle & Sargent 1972) remains the lowest-metallicity galaxy yet found,

despite 3 decades of searching. Low-metallicity galaxies have had little or no star formation up to the present epoch and are therefore of very low luminosity. As a result, most existing compilations of the MIR properties of galaxies are restricted to high-metallicity, high-luminosity targets (e.g., Genzel et al. 1998; Lu et al. 2003). Where low-metallicity galaxy spectra have been obtained, though, they differ dramatically from their higher-metallicity cousins in their infrared properties, with hotter large-grain dust emission and weak PAH emission (Sauvage et al. 1990; Calzetti et al. 2000; Galliano et al. 2003; Contursi et al. 2000; Thuan et al. 1999; Houck et al. 2004b; Roche et al. 1991; Madden 2002).

This work greatly expands the sample of low-metallicity galaxies observed in the infrared, to explore the effects of metallicity on the infrared properties of galaxies in a systematic way. The larger sample has allowed us to pinpoint the metallicity at which the transition from weak to strong PAH emission occurs.

2. OBSERVATIONS AND DATA REDUCTION

The new data presented here were obtained using IRAC and MIPS. The IRAC data are all standard pipeline reductions using the most recent versions available in the archive, ranging from 9.5.0 to 10.5.0. The MIPS data were reduced using the MIPS DAT (Data Analysis Tool; Gordon et al. 2005).

Photometry was performed using the “imexam” and “imstat” tasks in IRAF⁵. Most sources in the sample are compact; in general, apertures large enough to encompass all the flux were used for MIPS, while the standard aperture with a radius of 10 pixels (12 $''$) was used for IRAC, as suggested in the IRAC data handbook. For the extended galaxies, matching apertures that include the whole galaxy were used for MIPS and IRAC, and extended-source corrections have been applied to

¹ Steward Observatory, University of Arizona, Tucson, AZ 85721; cengelbracht@as.arizona.edu

² Jet Propulsion Laboratory, MC 264-767, 4800 Oak Grove Drive, Pasadena, CA 91109

³ Department of Physics and Astronomy, University of Wyoming, Laramie, WY 82071

⁴ Spitzer Science Center, California Institute of Technology, Pasadena, CA 91125

⁵ IRAF is distributed by the National Optical Astronomy Observatories, which are operated by the Association of Universities for Research in Astronomy, Inc., under cooperative agreement with the National Science Foundation.

the IRAC measurements as described in the IRAC data handbook. No color corrections were applied, which should not have a strong impact on the results since the corrections listed in the IRAC and MIPS handbooks are typically only a few percent.

To increase the number of metal-rich galaxies in the sample, we have supplemented our measurements with results from the literature. Where IRAC and MIPS measurements were available, they have been taken directly from the sources indicated in Table 1. We have synthesized IRAC and MIPS measurements from an IRS (Infrared Spectrograph; Houck et al. 2004a) measurement of NGC 7714 by Brandl et al. (2004) by convolving the spectrum with the IRAC $8\mu\text{m}$ and MIPS $24\mu\text{m}$ spectral response curves available on the SSC (*Spitzer* Science Center) website.

Finally, we have added several measurements from MSX (Midcourse Space Experiment) by Kraemer et al. (2002) and IRAS (Infrared Astronomical Satellite) by Rice et al. (1988). The MSX Band A ($8.28\mu\text{m}$) and IRAC $8\mu\text{m}$ flux densities measured for two galaxies (M 101, K. Gordon, in preparation; M 83, C. Engelbracht, in preparation) are very similar (within 20% in both cases), so we have made no correction to the MSX measurements used in this paper. We have made an empirical color correction from the IRAS $25\mu\text{m}$ band to the MIPS $24\mu\text{m}$ band by comparing the measured flux densities of NGC 7331 (Regan et al. 2004), M 81 (Gordon et al. 2004), NGC 55 (Engelbracht et al. 2004), and M 101 (K. Gordon, in preparation). The measured $24\mu\text{m}$ to $25\mu\text{m}$ ratios ranged from 0.81 to 0.94, so we applied the average value, 0.87, to all the IRAS measurements incorporated into the flux density ratio measurements in Table 1.

The resulting sample is a heterogeneous collection of star-forming galaxies without strong active nuclei. The global photometry measurements make this sample suitable for comparison to high-redshift samples (e.g., Fazio et al. 2004), where only flux measurements integrated over the whole galaxy are feasible. The metallicity quoted for each galaxy generally applies to a much smaller beam than for the infrared data. The outer regions of each galaxy should have lower metallicity than the nuclei. Thus, the beam mismatch would, if anything, weaken the trend of infrared properties we see clearly in the suite of measurements. We conclude it is not an impediment to this study.

3. RESULTS

To explore the contribution of PAH emission to the $8\mu\text{m}$ band, we compare the $8\mu\text{m}$ measurements to bands at both shorter and longer wavelengths. The longer-wavelength $24\mu\text{m}$ band is already dominated by emission by dust and so we use it directly, but the shorter-wavelength 5.8 and $4.5\mu\text{m}$ bands can contain significant contributions from PAH emission and starlight, respectively. To avoid contamination from PAH features, we do not use the $5.8\mu\text{m}$ band to derive the dust continuum measurement. We instead use the $4.5\mu\text{m}$ band, from which we subtract the stellar component as follows: We assume the $3.6\mu\text{m}$ band is dominated by starlight (which may result in an underestimate of the $4.5\mu\text{m}$ dust emission by a few percent; cf. Helou et al. 2004) and multiply the $3.6\mu\text{m}$ measurement by the $4.5/3.6\mu\text{m}$ ratio

expected for the stellar population, derived from Starburst99 (Leitherer et al. 1999) data files available on the web⁶. The ratio predicted by that model is typically 0.53 to 0.61, depending on star formation history and metallicity. We adopt the average value of 0.57 and assign to it an uncertainty of 7%. Hereafter, we refer to this ratio as α . Our adopted value of α is similar, but not identical to, the value of 0.47 in the template elliptical galaxy spectrum used by Lu et al. (2003) to measure the hot dust component in a sample of galaxies. This will have some effect on our measurement of the $4.5\mu\text{m}$ dust component for specific galaxies but does not affect the conclusions we draw from a diagnostic plot, as we discuss below. The scaled $3.6\mu\text{m}$ measurement is then subtracted from the $4.5\mu\text{m}$ measurement. For the galaxies in this sample, the scaled $3.6\mu\text{m}$ measurement ranges from 26% to 96% of the $4.5\mu\text{m}$ measurement, with an average value of 70%.

We did not subtract the stellar contribution from the $8\mu\text{m}$ and $24\mu\text{m}$ measurements because the correction is small for these galaxies and has no impact on our conclusions. Using the same Starburst99 models as above, we derive that the stellar contribution at $8\mu\text{m}$ ranges from 1% to 30% with an average of 10% and the contribution at $24\mu\text{m}$ is negligible, less than 1% on average.

The $8\mu\text{m}$ measurements compared to the short and long wavelength bands are summarized in Table 1, where the ratio to the $4.5\mu\text{m}$ band is referred to as R_1 and the ratio to the $24\mu\text{m}$ band as R_2 . Increasing levels of PAH emission will result in decreasing values of R_1 and increasing values of R_2 . We note that any correction for dust in the $3.6\mu\text{m}$ band will tend to increase the calculated $4.5\mu\text{m}$ dust emission and therefore increase the value of R_1 for those galaxies without strong PAH emission.

The color measurements are presented graphically in Figure 1. The figure shows that galaxies with high values of R_1 tend to have low values of R_2 , while those galaxies with a value of R_1 in the range of 0.01 to 0.09 (similar to our galaxy; cf. Lu 2004) tend to have larger values of R_2 , although with a large dispersion. We find that the separation of galaxies in this plot persists if we change our assumptions about how to compute the $4.5\mu\text{m}$ dust continuum, e.g., by changing the value of α to 0.47 to match the value used by Lu et al. (2003) or by using near-infrared data (such as the J band, which should not have a contribution from hot dust) to determine the stellar contribution to the $4.5\mu\text{m}$ band. This trend is consistent with the spectroscopic results summarized in the “PAH” column of Table 1, which demonstrate that all the galaxies with spectra free of PAH emission cluster in the upper-left portion of the diagram.

To interpret these results, we used the SED models of Dale et al. (2001a). To compute photometry from the models (which do not contain a stellar emission component), we convolved them with the same spectral response curves discussed in § 2. The various flux density ratios were then computed as for the data. The emission in the IRAC bands derived from these models is dominated by a fixed PAH spectral template, and as a result the models have a nearly constant value of R_1 , around 0.025. The models cover a range of R_2 values that depends on the temperature of the thermally puls-

⁶ <http://www.stsci.edu/science/starburst99/>

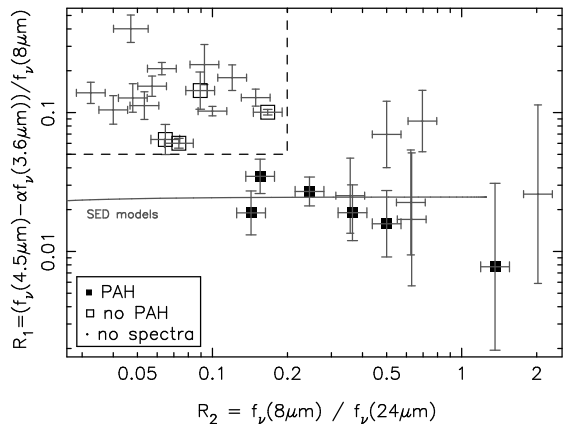


FIG. 1.— MIR colors of galaxies with a range of metallicities. The $8\mu\text{m}$ band is compared to both shorter ($4.5\mu\text{m}$, with stellar emission subtracted as described in the text) and longer ($24\mu\text{m}$) wavelengths. Galaxies with known PAH features are indicated by filled markers, while galaxies known to lack PAH features are indicated by open markers. Error bars include a 10% relative calibration uncertainty between the IRAC and MIPS instruments and a 7% uncertainty on α , in addition to photometric uncertainties. The dashed line indicates our chosen separation between PAH and non-PAH galaxies in this color space. The range of points covered by the Dale et al. (2001a) SED models is shown as a solid line.

ing grains, along the locus of points *outside* the region to the upper left occupied by the PAH-free galaxies. Thus, the weakness of the $8\mu\text{m}$ emission relative to the other bands appears to be due to the weakness of the PAH emission relative to the emission from small dust grains.

Figure 2 shows the 8-to- $24\mu\text{m}$ color vs. metallicity (the solar metallicity on this scale is 8.7; Allende Prieto et al. 2001). We label the galaxies according to the lack or presence of $8\mu\text{m}$ PAH emission using the color separation from Figure 1. They separate very cleanly according to metallicity, with a narrow transition region around 1/3 to 1/5 solar metallicity. One additional galaxy, NGC 1569, has been shown to have weak PAH emission (Lu et al. 2003) and has an O/H-based metallicity 25% of solar, consistent with this overall behavior.

The boundary between metallicities with and without PAH emission is surprisingly sharp, and it seems likely that future studies will show more scatter. For example, there can be significant variations in metallicity within these systems (e.g., a factor of three is indicated for SBS 0335-052; Houck et al. 2004b). Our characterization of this parameter with a single value is an oversimplification. In addition, “metallicity” includes enrichment of the ISM with a broad variety of elements, produced in different ways. Oxygen is produced predominantly in very massive stars; use of other elements produced in other ways as metallicity indicators may yield different behavior. Nonetheless, there is a robust trend toward low PAH emission in galaxies with relatively unpolluted ISMs.

Why do the PAH features become weaker in low-metallicity galaxies? We reject extinction as a possible cause, both because the effect would have to (counterintuitively) become stronger in galaxies with lower heavy-element abundance (and presumably less dust) and because the direct measurement of extinction in the low-metallicity galaxy SBS 0335-052 shows it to be optically

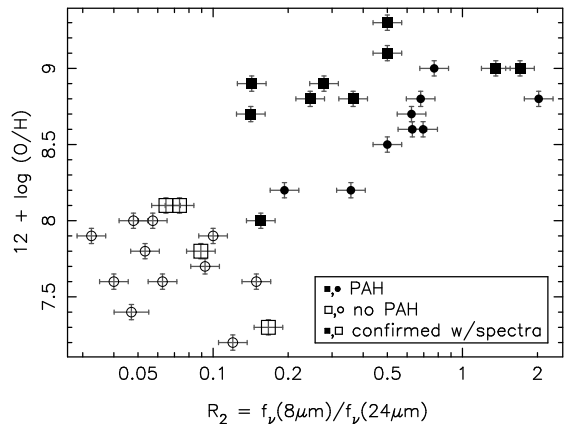


FIG. 2.— Galaxy metallicity as a function of the 8 to $24\mu\text{m}$ color. Galaxies with colors or spectra that indicate that they have $8\mu\text{m}$ PAH features are displayed as filled markers, while galaxies which lack the $8\mu\text{m}$ PAH feature are shown as open markers. Squares and circles denote measurements with and without spectroscopic confirmation, respectively. The error bars on the 8/ $24\mu\text{m}$ ratio are the same as in Figure 1, while the error bars on the metallicity are typically 0.05 or less (cf. Kobulnicky & Skillman 1996) and were all assigned an uncertainty of 0.05. Note that this figure does not require IRAC data (some of the $8\mu\text{m}$ measurements were made by MSX) and thus contains more points than Figure 1.

thin in the MIR (Houck et al. 2004b). It is also unlikely that starburst activity (i.e., the intensity of the star formation) is a major contributor to the effect: the correlation coefficient between R_2 and the $24\mu\text{m}$ surface brightness (an indicator of the specific star formation rate, which we estimated from the integrated flux densities and the visible extent of the galaxies in the sample) is much lower than the correlation coefficient between R_2 and the metallicity (0.26 vs. 0.79). Also, while the well-known starburst galaxies in our sample (e.g., NGC 253, NGC 7714), do tend to have lower R_2 values than other galaxies at similar metallicity, none of them have as small an R_2 value as the lowest metallicity galaxies. One possible reason is the destruction of the PAH carrier in the harsh radiation field of a low-metallicity galaxy (Plante & Sauvage 2002). Another possibility is that these galaxies are truly young and the PAH molecules have simply not had time to form (Dale et al. 2001b). For example, it is well known that the ISM of a galaxy must be significantly polluted with oxygen (produced copiously in very massive stars) before significant amounts of carbon are produced (by stars of a few M_\odot) — this effect may delay PAH production (E. Dwek, private communication). The low-metallicity galaxies may simply lack the carbon-rich AGB stars required to form the PAH molecules (Latter 1991).

In addition, we find that the PAH features included in the Dale et al. (2001a) models fail to account for the high values of R_1 prevalent at low metallicity (i.e., below 8.0). The emission by dust in the models below $10\mu\text{m}$ is several orders of magnitude lower than the emission from the PAH template (which does not vary), so the simple remedy to the models of weakening the PAH spectrum does not allow them to match the low-metallicity data. The value of R_1 derived from the model depends only on the shape of the PAH template spectrum and does not match the low-metallicity galaxies shown in Figure 1

(i.e., the model R_1 value plotted in Figure 1 does not shift as the PAH features are weakened). Some other source of emission must be dominating in these sources, such as hot dust in the $4.5\mu\text{m}$ band (cf. Lu et al. 2003).

4. CONCLUSIONS

We have combined new MIR measurements from the *Spitzer Space Telescope* with results from the literature to show that the $8\mu\text{m}$ to $24\mu\text{m}$ flux density ratio in star-forming galaxies depends strongly on metallicity. The $8\mu\text{m}$ to $24\mu\text{m}$ color changes markedly between 1/3 to 1/5 solar metallicity — the mean ratio below 1/3 solar metallicity is 0.08 ± 0.04 , while the ratio at higher metallicity is 0.70 ± 0.53 . A MIR color-color diagram which compares the $8\mu\text{m}$ band to dust continuum measurements at 4.5 and $24\mu\text{m}$ shows that the change in the ratio is predominantly due to a decrease in the $8\mu\text{m}$ emission. We interpret this result as a weakening of the PAH features at low metallicity, an interpretation consistent with the spectroscopic evidence available in the literature.

We show that existing empirical SED models cannot

account for the color change merely by weakening the PAH component of the models. In addition to the dependence of PAH strength on metallicity, SED models must account for another source of emission (e.g., hot dust) to explain the IRAC observations of low-metallicity galaxy colors.

The shift in 8 to $24\mu\text{m}$ ratio occurs at a fairly high metallicity and will thus affect the spectra of many galaxies. Future SED models to interpret *Spitzer* measurements at high redshift must take the dependence of metallicity on redshift into account.

We thank Eli Dwek for helpful discussions, and Nanyao Lu and Eiichi Egami for comments which improved this paper. This work is based in part on observations made with the *Spitzer Space Telescope*, which is operated by the Jet Propulsion Laboratory, California Institute of Technology under NASA contract 1407. Support for this work was provided by NASA through Contract Number 960785 issued by JPL/Caltech.

REFERENCES

- Allende Prieto, C., Lambert, D. L., & Asplund, M. 2001, *ApJ*, 556, L63
- Bergvall, N. & Östlin, G. 2002, *A&A*, 390, 891
- Brandl, B. R., et al. 2004, *ApJS*, 154, 188
- Calzetti, D., Armus, L., Bohlin, R. C., Kinney, A. L., Koornneef, J., & Storchi-Bergmann, T. 2000, *ApJ*, 533, 682
- Cesarsky, D., Lequeux, J., Pagani, L., Ryter, C., Loinard, L., & Sauvage, M. 1998, *A&A*, 337, 35
- Chary, R., et al. 2004, *ApJS*, 154, 80
- Contursi, A., et al. 2000, *A&A*, 362, 310
- Dale, D. A., Helou, G., Contursi, A., Silbermann, N. A., & Kolhatkar, S. 2001a, *ApJ*, 549, 215
- Dale, D. A., Helou, G., Neugebauer, G., Soifer, B. T., Frayer, D. T., & Condon, J. J. 2001b, *AJ*, 122, 1736
- Devost, D., et al. 2004, *ApJS*, 154, 242
- Engelbracht, C. W., et al. 2004, *ApJS*, 154, 248
- Fazio, G. G., et al. 2004, *ApJS*, 154, 39
- Galliano, F., Madden, S. C., Jones, A. P., Wilson, C. D., Bernard, J.-P., & Le Peintre, F. 2003, *A&A*, 407, 159
- Garnett, D. R. 2002, *ApJ*, 581, 1019
- Genzel, R., et al. 1998, *ApJ*, 498, 579
- Gordon, K. D., et al. 2005, *PASP*, in press
- Gordon, K. D., et al. 2004, *ApJS*, 154, 215
- Guseva, N. G., Izotov, Y. I., & Thuan, T. X. 2000, *ApJ*, 531, 776
- Heckman, T. M., Robert, C., Leitherer, C., Garnett, D. R., & Van der Rydt, F. 1998, *ApJ*, 503, 646
- Helou, G., et al. 2004, *ApJS*, 154, 253
- Hinz, J. L., et al. 2004, *ApJS*, 154, 259
- Houck, J. R., et al. 2004a, *ApJS*, 154, 18
- Houck, J. R., et al. 2004b, *ApJS*, 154, 211
- Izotov Y. I., Thuan, T. X., & Lipovetsky, V. A. 1997, *ApJS*, 108, 1
- Izotov Y. I. & Thuan, T. X. 1999, *ApJ*, 511, 639
- Kniazev, A. Y., et al. 2000, *A&A*, 357, 101
- Kobulnicky, H. A. & Skillman, E. D. 1996, *ApJ*, 471, 211
- Kobulnicky, H. A., Kennicutt, R. C., Jr., & Pizagno, J. L. 1999, *ApJ*, 514, 544
- Kraemer, K. E., Price, S. D., Mizuno, D. R., & Carey, S. J. 2002, *AJ*, 124, 2990
- Kunth, D. & Joubert, M. 1985, *A&A*, 142, 411
- Kunth, D. & Östlin, G. 2000, *A&A Rev.*, 10, 1
- Lagache, G., et al. 2004, *ApJS*, 154, 112
- Latter, W. B. 1991, *ApJ*, 377, 187
- Leitherer, C., et al. 1999, *ApJS*, 123, 3
- Liang, Y. C., Hammer, F., Flores, H., Elbaz, D., Marcillac, D., & Cesarsky, C. J. 2004, *A&A*, 423, 867
- Lisenfeld, U. & Ferrara, A. 1998, *ApJ*, 496, 145
- Lu, N., et al. 2003, *ApJ*, 588, 199
- Lu, N. 2004, *ApJS*, 154, 286
- Madden, S. C. 2002, *Ap&SS*, 281, 247
- Marleau, F., et al. 2004, *ApJS*, 154, 66
- Masegosa, J., Moles, M., & Campos-Aguilar, A. 1994, *ApJ*, 420, 576
- Pahre, M. A., Ashby, M. L. N., Fazio, G. G., & Willner, S. P. 2004, *ApJS*, 154, 235
- Papovich, C., et al. 2004, *ApJS*, 154, 70
- Plante, S. & Sauvage, M. 2002, *AJ*, 124, 1995
- Regan, M. W., et al. 2004, *ApJS*, 154, 204
- Rice, W., Lonsdale, C. J., Soifer, B. T., Neugebauer, G., Koplan, E. L., Lloyd, L. A., de Jong, T., & Habing, H. J. 1988, *ApJS*, 68, 91
- Rigopoulou, D., Spoon, H. W. W., Genzel, R., Lutz, D., Moorwood, A. F. M., & Tran, Q. D. 1999, *AJ*, 118, 2625
- Roche, P. F., Aitken, D. K., & Ward, M. J. 1991, *MNRAS*, 248, 606
- Sauvage, M., Vigroux, L., & Thuan, T. X. 1990, *A&A*, 237, 296
- Searle, L. & Sargent, W. L. W. 1972, *ApJ*, 173, 25
- Smith, J. D. T., et al. 2004, *ApJS*, 154, 199
- Storchi-Bergmann, T., Calzetti, D., & Kinney, A. L. 1994, *ApJ*, 429, 572
- Thuan, T. X., Sauvage, M., & Madden, S. 1999, *ApJ*, 516, 783
- Willner, S. P., et al. 2004, *ApJS*, 154, 222
- Yan, L., et al. 2004, *ApJ*, 154, 60

TABLE 1
GALAXY COLORS AND METALLICITIES

Galaxy	$f_{\nu}(4.5\mu\text{m})$ Jy	$f_{\nu}(24\mu\text{m})$ Jy	R_1^a	R_2^b	Z^c	PAH ^d	References flux densities ^e	Z	PAH
I Zw 18	3.4e-4	5.5e-3	0.18	0.12	7.2	...	1	2	...
SBS 0335-052	1.5e-3	6.6e-2	0.10	0.17	7.3	no	1	3	4
HS 0822+3542	1.45e-4	2.7e-3	0.40	0.06	7.4	...	1	5	...
Tol 1214-277	7.2e-5	5.5e-3	0.10	0.04	7.6	...	1	2	...
Tol 65	3.6e-4	1.5e-2	0.21	0.06	7.6	...	1	2	...
Tol 2138-405	2.4e-3	5.7e-2	0.13	0.15	7.6	...	1	6	...
VII Zw 403	2.4e-3	2.8e-2	0.22	0.09	7.7	...	1	7	...
Mrk 153	1.45e-3	2.9e-2	0.14	0.08	7.8	no	1	8	9
UM 461	5.5e-4	3.0e-2	0.11	0.05	7.8	...	1	2	...
Haro 11	3.2e-2	1.9e+0	0.10	0.10	7.9	...	1	10	...
NGC 4861	3.2e-3	2.8e-1	0.14	0.03	7.9	...	1	11	...
Mrk 1450	9.2e-4	4.8e-2	0.13	0.05	8.0	...	1	12	...
UM 448	1.1e-2	5.6e-1	0.03	0.16	8.0	yes	1	12	9
UM 462	2.4e-3	1.1e-1	0.15	0.06	8.0	...	1	2	...
Mrk 930	2.3e-3	1.7e-1	0.06	0.06	8.1	no	1	12	9
II Zw 40	1.1e-2	1.5e+0	0.06	0.07	8.1	no	1	2	13
NGC 4670	1.5e-2	2.1e-1	0.03	0.36	8.2	...	1	14	...
NGC 1156	...	4.5e-1	...	0.19	8.2	...	15	16	...
NGC 0598	...	5.0e+1	...	0.50	8.5	...	17,18	19	...
NGC 3077	2.76e-1	1.5e+0	0.02	0.48	8.6	...	1	20	...
NGC 300	8.8e-1	2.3e+0	0.09	0.70	8.6	...	21	19	...
NGC 2537	4.1e-2	2.4e-1	0.02	0.62	8.7	...	1	22	...
NGC 7714	...	2.4e+0	...	0.14	8.7	yes	23	20	23
NGC 2782	3.8e-2	9.6e-1	0.02	0.36	8.8	yes	1	14	24
NGC 4194	6.5e-2	3.1e+0	0.03	0.25	8.8	yes	1	20	25
NGC 5457	...	1.0e+1	...	0.68	8.8	...	26	19	...
NGC 3031	6.5e+0	4.4e+0	0.03	2.02	8.8	...	27,28	19	29
He 2-10	6.0e-2	4.9e+0	0.02	0.14	8.9	yes	1	11	24
NGC 253	...	1.4e+2	...	0.28	8.9	yes	17,30	19	31
NGC 5055	...	6.1e+0	...	0.77	9.0	...	17,30	19	...
NGC 7331	9.5e-1	3.6e+0	0.01	1.36	9.0	yes	32	19	33
NGC 224	...	9.4e+1	...	1.70	9.0	yes	17,30	19	34
NGC 5236	...	4.2e+1	...	0.50	9.1	yes	1,30	19	29
NGC 2903	1.2e-1	2.2e+0	0.02	0.50	9.3	yes	1	11	9

REFERENCES. — (1) This paper; (2) Kobulnicky & Skillman (1996); (3) Izotov & Thuan (1999); (4) Houck et al. (2004b); (5) Kniazev et al. (2000); (6) Masegosa et al. (1994); (7) Izotov et al. (1997); (8) Kunth & Joubert (1985); (9) Engelbracht et al., in preparation; (10) Bergvall & Östlin (2002); (11) Kobulnicky et al. (1999); (12) Guseva et al. (2000); (13) Madden (2002); (14) Heckman et al. (1998); (15) Pahre et al. (2004); (16) Lisenfeld & Ferrara (1998); (17) MSX Band A measurements by Kraemer et al. (2002); (18) Hinz et al. (2004); (19) Garnett (2002); (20) Storchi-Bergmann et al. (1994); (21) Helou et al. (2004); (22) J. Moustakes, private communication; (23) IRS spectroscopy by Brandl et al. (2004) convolved with IRAC and MIPS response curves as described in the text; (24) Roche et al. (1991); (25) Lu et al. (2003); (26) K. Gordon, in preparation; (27) Willner et al. (2004); (28) Gordon et al. (2004); (29) Rigopoulou et al. (1999); (30) IRAS measurements by Rice et al. (1988) transformed to MIPS 24 μm measurements as described in the text; (31) Devost et al. (2004); (32) Regan et al. (2004); (33) Smith et al. (2004); (34) Cesarsky et al. (1998).

^a $R_1 = [f_{\nu}(4.5\mu\text{m}) - \alpha f_{\nu}(3.6\mu\text{m})]/f_{\nu}(8\mu\text{m})$, where α is as described in the text.

^b $R_2 = f_{\nu}(8\mu\text{m})/f_{\nu}(24\mu\text{m})$

^c $12 + \log(O/H)$

^dThe PAH designation is based on results reported in the cited works or on visual inspection of the spectra.

^eA single entry refers to both IRAC and MIPS measurements together. Two entries indicate separate sources for the measurements, with the IRAC reference followed by the MIPS reference.